Monthly Notices
of the
ROYAL ASTRONOMICAL SOCIETY

MNRAS **437,** 316–326 (2014)
Advance Access publication 2013 October 31

doi:10.1093/mnras/stt1886

The soft component and the iron line as signatures of the disc inner radius in Galactic black hole binaries

Mari Kolehmainen,[1,2]⋆ Chris Done[2] and María Díaz Trigo[3]

[1]*School of Physics & Astronomy, University of Southampton, Highfield, Southampton SO17 1BJ, UK*
[2]*Department of Physics, University of Durham, South Road, Durham DH1 3LE, UK*
[3]*European Southern Observatory, ALMA Regional Centre, Karl-Schwarzschild-Str. 2, D-85748 Garching, Germany*

Accepted 2013 October 2. Received 2013 September 20; in original form 2013 March 7

ABSTRACT

The inner radius of the accretion disc around a black hole in the low/hard state can be measured in one of two ways. First, via the extent of broadening of the iron emission line, and secondly, from the luminosity and temperature of the weak soft component seen in this state, assuming it is the disc. We use both of these methods on all the low/hard state spectra taken in timing mode of *XMM–Newton*'s EPIC-pn. We find that the two methods are not consistent with each other, and the difference is not always in a single direction. The two methods are neither model independent, nor are they independent of current calibration issues. We find that the remaining small residuals in the EPIC-pn timing mode response at the $\leq$3 per cent level can have a dramatic effect on the fit parameters for the reflected spectrum. There is also a mismatch in cross-calibration with *RXTE*, which makes it difficult to use simultaneous data to extend the bandpass of the spectral fits. Nonetheless, it is clear from the data that the iron line is noticeably broader and stronger at higher $L/L_{\rm Edd}$, which is consistent with the truncated disc models. We also show that it is likely that the soft component changes character, from a stable component consistent with a truncated disc at high $L/L_{\rm Edd}$, to a variable one with much smaller radius at low $L/L_{\rm Edd}$. This adds to growing evidence for a complex soft component in the low/hard state, possibly resulting from clumps torn from the edge of the truncated disc.

Key words: accretion, accretion discs – black hole physics – X-rays: binaries.

1 INTRODUCTION

The current paradigm for the structure of the accretion flow in black hole binaries (hereafter BHB) at low luminosities is that the cool, optically thick, geometrically thin standard accretion disc is progressively replaced in the inner regions by a hot, optically thin, geometrically thick flow as the mass accretion rate decreases (low/hard state; Esin, McClintock & Narayan 1997). This model has gained widespread acceptance by its ability to provide a framework in which to interpret large amounts of apparently unrelated observational data, predominantly revealed by the multiple *RXTE* observations of these systems. At the lowest luminosities, the large disc truncation radius means that the disc emission is cool and dim. Few seed photons from the disc illuminate the flow, so the Comptonized spectra are hard. Decreasing the disc truncation radius leads to a stronger disc component, and to a greater overlap of the flow with the disc. This gives more seed photons to Compton cool the flow, giving softer Compton spectra. The decreasing radius also means that any frequencies set by this radius will increase, giving a qualitative description of the increasing characteristic frequencies seen in the power spectra and their tight correlation with the energy spectra. The flow is completely replaced by the disc when the disc reaches its minimum radius of the last stable circular orbit (high/soft state), giving a physical mechanism for the marked hard-to-soft transition seen in BHBs. Even the jet behaviour can be tied into this picture, as a large-scale height flow is probably required for jet formation, so the collapse of the inner flow as the disc reaches its minimum radius triggers a similar collapse of the radio emission [see e.g. Fender, Belloni & Gallo 2004, and the reviews by McClintock & Remillard (2006) and Done, Gierliński & Kubota (2007), hereafter DGK07].

Despite these evident successes, these models remain controversial due to reports that the disc extends down to the last stable orbit in the low/hard state. There are two observational signatures of this. First, reflection of the Comptonized emission from the disc is smeared by a combination of special and general relativistic effects, and the extent of this broadening is determined by the inner disc radius (e.g. the review by Fabian et al. 2000). Secondly, the luminosity and temperature of the direct continuum from the disc itself can be used to evaluate the emitting area, and hence the inner disc radius. Both these require CCD data rather than the more numerous proportional counter *RXTE* data sets (lower energy bandpass for

⋆ E-mail: mari.kolehmainen@soton.ac.uk

the low temperature disc emission, and higher spectral resolution for the iron line profile). A recent review of low/hard state CCD spectra from BHB by Reis, Fabian & Miller (2010, hereafter R10) noted that both these signatures were routinely seen at a level which generally excluded a truncated disc.

These reports are themselves controversial, and have been challenged in literature. The most convincing broad iron line profile in R10 is from a bright low/hard state of GX 339−4. This profile is derived from data where instrumental pileup is an issue (Miller et al. 2006; Done & Díaz Trigo 2010). Simultaneous data from another instrument which does not suffer from pileup clearly show a much narrower line (Done & Díaz Trigo 2010). However, simulations of pileup do not produce an artificially broad line (Miller et al. 2010), but our understanding of pileup for such an extreme count rate (200× over the limit for the instrument mode used) is probably not complete (see also counterexamples in the data compilations of Ng et al. 2010; Yamada et al. 2009).

The intrinsic disc emission has a different set of issues. First it can be much weaker than the Compton continuum even in the CCD X-ray bandpass, so its luminosity and temperature depend on how the continuum is modelled (e.g. the difference in inner radius in Rykoff et al. 2007, from using Comptonized emission compared to a power law). This is unlike the situation in the high/soft state, where the disc dominates and the high energy continuum model has little effect on the results (e.g. Kubota & Done 2004). Even having modelled the disc emission, its luminosity and temperature need not be simply due to gravitational energy release as in the high/soft state. X-ray heating from illumination by the much stronger hard X-ray component can change the derived inner disc radius from being consistent with the last stable orbit (Rykoff et al. 2007) to being considerably larger, especially as the standard stress-free inner boundary condition is probably not appropriate for a truncated disc (Gierliński, Done & Page 2008).

However, it is also possible that the disc is considerably more complex. First, even disc dominated high/soft spectra are not completely described by current disc models. They are broader than a simple sum of blackbodies, as expected due to relativistic smearing, and fit much better to models which incorporate this as well as full radiative transfer through the disc photosphere. While this makes a very nice physical picture, the disc spectra are even better fit by phenomenological models, showing the limitations of the best current theoretical descriptions of disc spectra (Kubota et al. 2010; Kolehmainen, Done & Díaz Trigo 2011). Secondly, the disc need not be a single structure. The inner edge of the truncated disc is not likely to be smooth. Clumps torn off the disc edge will spiral inwards into the hot flow, so will heat up by thermal conduction and evaporate. Before they completely merge into the hot flow they can form a small area, hotter, soft component, separate from the main body (and spectrum) of the truncated disc itself [see figs 9 and 10 in Chiang et al. (2010), Yamada et al. 2013].

As well as potential complexity of the disc spectrum, there is also potential complexity of the Compton continuum. At low luminosities the hot flow should be quite optically thin, in which case Compton scattering gives a bumpy rather than smooth power-law spectrum. At higher luminosities the flow has higher optical depth, so can be inhomogeneous, with different parts of the flow giving different Comptonized spectra. This is required in order to produce the observed spectral lags, where the soft continuum varies before the harder continuum (Miyamoto et al 1988; Kotov, Churazov & Gilfanov 2001; Arévalo & Uttley 2006). Even more direct evidence for this is seen in the frequency resolved spectra, where the most rapidly variable parts of the flow (few tens of milliseconds, presumably the inner regions) have harder spectra and less reflection than the more slowly variable emission (few seconds, presumably the outer parts of the flow: Revnivtsev, Gilfanov & Churazov 1999; Axelsson, Hjalmarsdotter & Done 2013). This gives rise to spectral curvature, which can be seen in broad-band data (Di Salvo et al. 2001; DGK07; Makishima et al. 2008; Kawabata & Mineshige 2010; Shidatsu et al. 2011; Yamada et al. 2013). Fitting such continuua with a single Comptonization component leads to a requirement for an additional soft component, but this is connected to the Comptonization region rather than to the disc.

Thus, there is controversy both from instrumental effects for these bright sources (iron line), and over the physical interpretation of what is seen (origin of the soft X-ray component). We pick one particular instrument configuration, that of *XMM–Newton* timing mode, as this is specifically designed to observe bright sources, and systematically examine all low/hard state spectra taken in this mode to date. We assess the effects of both instrumental and modelling uncertainties, and show that both the iron line and intrinsic disc emission can be consistent with the truncated disc models in all current low/hard state spectra.

2 OBSERVATIONS AND DATA ANALYSIS OVERVIEW

Galactic BHBs are generally too bright to be observed in the standard imaging modes of CCD detectors, even in the low/hard state. We are therefore restricted to fast timing modes, which are currently less well calibrated than the standard imaging modes usually used for fainter sources. We select the EPIC-pn timing mode of *XMM–Newton*, as this is the mode which normally maximizes the non-piled up count rate for low/hard state BHB.

There are seven archival observations of canonical low/hard states from four sources in this mode: Cygnus X-1, Swift J1753−0127, GX 339−4 (four data sets) and H1743−322. The latter object has an interstellar column density of $\sim 10^{22}$ cm^{-2}, substantially higher than the others. This means that the low energy continuum emission in H1743−322 is much less visible. This clearly reduces the constraint on the intrinsic disc emission, but also affects the iron line, as the latter depends on accurate modelling of the continuum emission underneath the line (see e.g. Kolehmainen et al. 2011), which in turn requires broad bandpass data. Thus we exclude H1743−322 from this analysis (see Table 1). We also considered the single archival observation of a recently discovered black hole candidate XTE J1752−223 (Markwardt et al. 2009), which caught the source

Table 1. Details of the *XMM–Newton* observations analysed in this paper. The highly-absorbed BHB H1743−322 ($N_{\rm H} \sim 16 \times 10^{21}$) was excluded due to the absorption's obscuring effect at low energies. The binary parameters used in this paper are Cygnus X-1: $M = 20\,{\rm M}_{\odot}$, $D = 24$kpc, $i = 30^{\circ}$, GX 339−4: $M = 10\,{\rm M}_{\odot}$, $D = 8$kpc, $i = 60^{\circ}$ and Swift J1753: $M = 9\,{\rm M}_{\odot}$, $D = 6$ kpc, $i = 60^{\circ}$.

	Obsid	cts s^{-1}[a]	Exp (s)
Cygnus X-1	0602610401	479 ± 0.4 (1111)	19 970
GX 339−4 (GX4)	0654130401	362 ± 0.3 (944)	25 290
GX 339−4 (GX3)	0204730301	257 ± 0.2	44 360
GX 339−4 (GX2)	0204730201	240 ± 0.2	30 480
GX 339−4 (GX1)	0605610201	125 ± 0.1	31 750
Swift J1753−0127	0311590901	85 ± 0.1	40 110

[a]The measured count rates. The values in brackets indicate original count rates before pile-up correction.

towards the end of a soft-to-hard state transition. However, on closer look the spectral shape of the observation resembles more that of a hard–intermediate state spectrum, which was also confirmed by the hardness-intensity and rms-properties of simultaneous *RXTE* observations. Thus, since this observation is not in the *canonical* low/hard state, it was omitted from our analysis.

The data were reduced using the *XMM–Newton* Science Analysis System (SAS) v10.0. We applied the standard data reduction expressions, using single and double events and ignoring bad pixels. All data were extracted in full RAWY [1:200] and RAWX of six rows on either side of the central row. The SAS tool EPATPLOT was used to check for pile-up in all of the observations. This showed that Cyg X-1 and the brightest low/hard state observation of GX 339−4 were slightly affected. This was corrected by excluding one row in RAWX on both sides of the peak of the emission. Response and ancillary files were generated with SAS tasks RMFGEN and ARFGEN, respectively. The spectra were then rebinned using SPECGROUP, with an oversampling factor of 3, as recommended for all of the EPIC detectors. Each bin was also set to have a minimum of 25 counts, and a systematic error of 1 per cent was added to the spectrum.

The current level of EPIC instrument calibration is discussed at length in the latest version of the *XMM–Newton* Calibration Technical Note (0083).[1] The main issue for concern is the ubiquitous problem of X-ray loading (XRL) in observations taken before 2012 May. The 'quiet' level of the electron current in each pixel is determined from exposures at the beginning of each observation, and this offset map is automatically subtracted from the data by the onboard processor. However, for bright sources, and especially bright, hard sources, this electron current is contaminated by the source itself. The source pixels have too much electron current subtracted, leading to an offset in the gain for each observation. However, as of 2012 May 30, the filter is closed at the start of each observation and the effect is not present in observations after this date. The newly published SAS13.0 also includes a task for correcting for the effects of XRL in the standard imaging mode, but not the fast timing modes.

The charge transfer inefficiency (CTI) is a separate issue, and does not include the effects of XRL. Damage to the CCD means that there are electron traps, so not all charge is transferred on readout. This CTI is reduced for bright sources, as the multiple electrons produced by high X-ray illumination fill the holes, so that the remaining charge can be efficiently transferred. This is currently corrected by the SAS task EPFAST, but the parameters for the gain shift were derived assuming that the data were affected only by a linear gain shift, while in reality they are affected by a combination of a linear gain shift from CTI and a constant offset from XRL. We follow current recommendations and use EPFAST on all our data, but at these relatively low count rates (compared to the ones seen in burst mode) the correction did not cause any noticeable changes in the data.

The wings of the point-spread function (PSF) of the EPIC-pn extend further than the data collection region in timing mode, which means that selecting a source-free region for background subtraction is not possible (e.g. Done & Díaz Trigo 2010). However, the 10–15 keV light curve from the outer regions of the EPIC-pn can still be used to identify and exclude periods of background flaring, and these can be checked from outer chip light curves from the MOS imaging data, when available. We also use blank sky backgrounds in timing mode to check that the background is indeed negligible for these bright, hard sources. Table 1 shows the resulting effective exposure time after excluding period of background flaring.

We also extract the quasi-simultaneous *RXTE* data on all of our objects and reduce these using standard methods. Table 1 gives details of the observations used.

[1] http://xmm.vilspa.esa.es/external/xmm_sw_cal/calib/documentation.shtml

3 LOW/HARD SPECTRA OVERVIEW

We start by fitting the data with a single power-law model to illustrate any possible deviations from a pure power-law continuum. Fig. 1 shows the data unfolded with this model and fitted in the 3–10 keV band. For plotting purposes we have divided Cyg X-1 and Swift J1753−0127 (hereafter S1753) by $(M/10)(8/D)^2$ so that the spectra are roughly normalized in relative $L/L_{\rm Edd}$ assuming that GX 339−4 is a $10{\rm M}_{\odot}$ black hole at 8 kpc.

The data show a clear trend in luminosity. At the lowest luminosities (S1753 in Fig. 1) the spectrum shows no clear features or deviations from a simple power-law continuum. At higher luminosities the excess emission around the iron line region increases in both strength and width with increasing $L/L_{\rm Edd}$. This effect is even more pronounced in Fig. 2, where the data are modelled with an absorbed power law in the 0.7–10 keV range and plotted as a data/model ratio. The hydrogen column density is let to vary within reasonable limits. The increasing soft excess at ∼1 keV is now also clearly visible. Assuming that this soft excess is the true disc component, these features are qualitatively consistent with the predictions of the standard truncated disc model. At the lowest luminosities the inner disc is truncated far from the last stable orbit, then subsequently reaching further inwards and becoming stronger as the source gets brighter. The reflection fraction also increases with luminosity, which could at least partially explain the change in the continuum shape above the broad iron line region in the brightest observation (GX4). We explore different explanations for this in Section 4 and further in the paper.

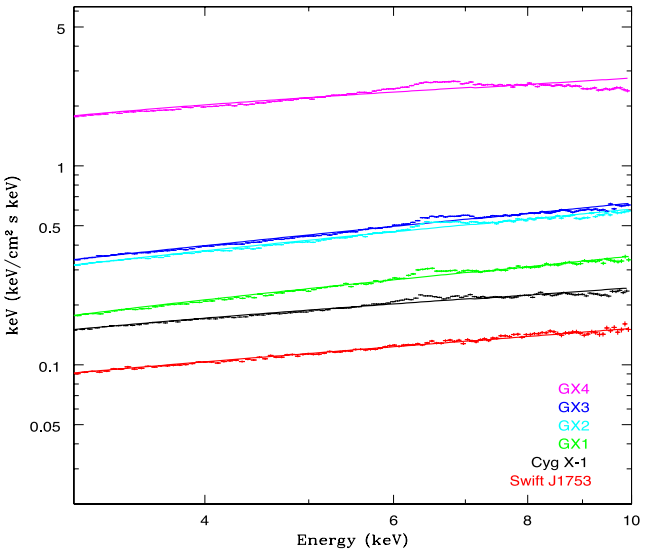

Figure 1. All the observations analysed in this paper, unfolded by a simple power-law model to illustrate the spectral deviations from a simple continuum. The spectra are plotted in order of increasing luminosity in the 3–10 keV range.

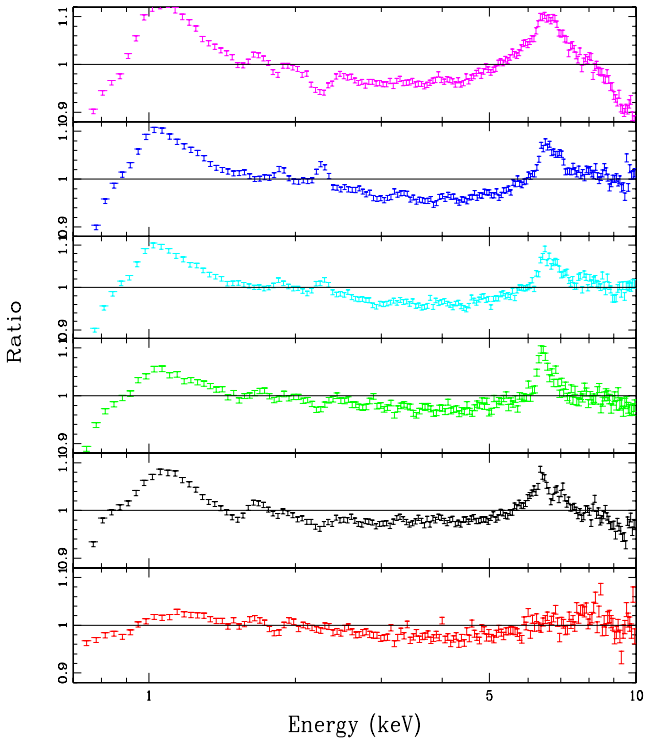

Figure 2. The data/model ratio of all the observations using absorbed power law in the 0.7–10 keV range., with the same colour convention as in Fig. 1. The data plotted in order of increasing luminosity to illustrate the changes in the soft excess and the iron line.

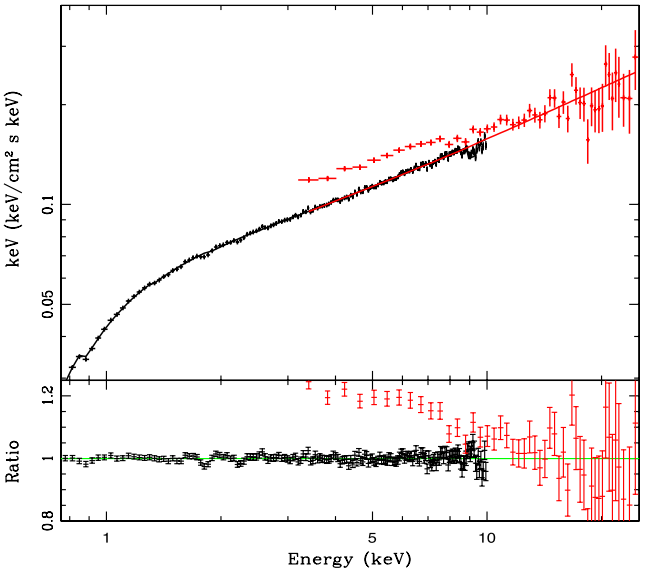

Figure 3. Joint EPIC-pn-PCA fit of the S1753 observation fitted in the joint energy range of 0.7–25 keV. The data are consistent only above 7 keV, with the difference in photon indices of $\Delta\Gamma \sim 0.11$. Due to this obvious disagreement in cross-correlation, the rest of this analysis focuses solely on the EPIC-pn data.

3.1 Cross-calibration with RXTE

As the EPIC-pn energy band only reaches up to 10 keV, we initially combine it with data from the *RXTE* PCA to cover more of the hard X-ray tail. However, fitting data from the two instruments showed an inconsistency in their cross-calibration. We demonstrate this with S1753, which has the simplest spectrum of our sample, with very little spectral features or curvature (see Figs 1 and 2). Fig. 3 shows the simultaneous EPIC-pn/PCA data of the same source. This shows a clear discrepancy in the cross-calibration of the two instruments in the region of overlap (3–10 keV). This was also noted in Hiemstra et al. (2011) for the bright BHB XTE J1652. However, for S1753 there is almost no spectral complexity to mask the issues. The two instruments clearly have different spectral indices, with $\Delta\Gamma = 0.11^{+0.01}_{-0.02}$, even restricting the fit to the 3–10 keV region where the data overlap. We find similar discrepancies in spectral indices in all our data in the overlapping 3–10 keV bandpass, though here the evident complexity around the iron line could affect the modelling. This issue was also noted in the latest update to the *XMM–Newton* Calibration Technical Note (v.1.6 of TN-0083), where the comparison was made between *RXTE*/PCA and the EPIC-pn burst mode, rather than timing mode (see also the Appendix). Even though the EPIC-pn science modes are different, the discrepancy is in the same direction, i.e. the PCA spectra are softer than the EPIC-pn.

Thus, it is clear that these data are still somewhat limited by calibration, and understanding these limitations and their origin is essential before making interpretations of such data. This offset in spectral index means that we cannot fit the EPIC-pn and the PCA data together. This is a general problem with cross-calibration between the two detectors, rather than a feature of timing mode alone (see the Appendix for the same issue in Burst and Imaging mode). Hence we focus the rest of this analysis solely on the EPIC-pn data, as we are primarily interested in the soft continuum and the iron line profile.

4 LOWEST $L/L_{\rm Edd}$: SWIFT J1753−0127

We start the more detailed analysis with the simplest spectrum, S1753. Previous work on this spectrum has shown that there is curvature in the continuum, which can be described either by a disc component or by reflection (R10; Hiemstra et al. 2011). However, both of these would imply that the inner disc is present at some level, in conflict with the simplest truncated disc model.

We confirm that there is indeed spectral curvature by fitting a series of models of increasing complexity. We start with a single Comptonization component, described by the NTHCOMP model of Zdziarski, Johnson & Magdziarz (1996), as a power law is a poor approximation for Comptonization where the bandpass is close to the seed photons. We assume these seed photons have a blackbody shape, and fix the electron temperature at 100 keV. We absorb this continuum so the total model is TBABS*NTHCOMP, giving $\chi^2_\nu = 196/163$ for a seed photon temperature of ∼0.2 keV. We add a disc spectrum with inner disc temperature tied to the seed photon temperature for Comptonization i.e. TBABS*(DISKBB+NTHCOMP). This gives a significantly better fit with $\chi^2 = 169/162$. The disc normalization of 400^{+180}_{-100} implies an apparent radius of 17 km for the fiducial values of distance and inclination. This gives a corrected radius of 20 km for a colour correction factor of 1.7 and stress free inner boundary condition of 0.41 (Kubota et al. 1998), which is $1.3R_g$ for the fiducial mass of 10 $M_\odot$. Even without the stress free inner boundary the radius is only $3R_g$, so this is completely inconsistent with a truncated disc. Instead, this small emitting area could be indicative of small clumps at large radii torn from the truncated disc edge, heated by conduction as they spiral into the hot flow (Chiang et al. 2010).

Instead, we get an even better fit using the EQPAIR Comptonization model with no additional soft component ($\chi^2_\nu = 160/163$). This model calculates the full Comptonized emission from each individual Compton scattering order, so at low optical depths and high temperatures (best fit is $\tau \sim 0.3$, $kT_e = 300$ keV) the excess soft X-ray flux is fit by the first order scattering from seed photons from the disc at 11 ± 1 eV. The disc normalization is completely unconstrained at these low temperatures, so is consistent with a truncated disc.

Thus the *spectrum* of S1753 is consistent within current instrumental uncertainties as being simply described by a single Comptonization continuum from low optical depth material, with no disc required in either direct or reflected emission, as predicted by the truncated disc models at low $L/L_{\rm Edd}$. However, this is not consistent with the *timing* behaviour. Fast time variability shows clearly that there *is* an additional component at soft energies (fig. 3 in Uttley et al. 2011). This soft component leads the harder X-rays by ∼0.1 s, far too long to be the light crossing time lags between individual Compton scattering orders (see also Miyamoto et al. 1988). Instead, these almost certainly are viscous lags from propagating fluctuations, with fluctuations in a spectrally softer component at larger radii propagating down to modulate a harder component produced at smaller radii (Kotov et al. 2001; Arévalo & Uttley 2006).

Hence we do want to include a separate soft component in the *XMM–Newton* bandpass in these data. If this is roughly blackbody in shape then it could either represent the inner edge of an untruncated disc around an extreme spin black hole, or small clumps torn from the edge of a disc which is truncated at much larger radii. Clumps have the advantage of also giving a clear origin for variability, whereas a disc down to the last stable orbit in the disc dominated states has remarkably little variability (e.g. Churazov, Gilfanov & Revnivtsev 2001).

Observationally, these two possibilities predict different reflection signatures. Small clumps subtend very little solid angle, so give a small reflected spectrum which is not strongly smeared. Conversely, an inner disc round a high spin black hole should be physically close to the X-ray source, so should give a larger reflected fraction and strong relativistic smearing. We include reflection of the Comptonization continuum from ionized material, modelled using the RFXCONV model, based on the tables of Ross & Fabian (2005) recoded as a convolution model (Kolehmainen et al. 2011). This is relativistically smeared using the Kerr metric transfer functions of Laor (1991), recoded as a convolution model. Thus the total model is TBABS*(DISKBB+NTHCOMP+KDBLUR*RFXCONV*NTHCOMP), and this gives $\chi^2_\nu = 140/159$, $\Delta\chi^2 = 25$ for three additional parameters better than the original DISKBB+NTHCOMP continuum model. The disc normalization is now allowed to be much larger, up to 2400, but this does not make the model compatible with a truncated disc as the reflected emission requires strong relativistic smearing, with $r_{\rm in} = 1.9^{+6.9}_{-0.6} R_g$ even though the amount of reflection is small ($\Omega/2\pi = 0.06^{+0.04}_{-0.02}$). The reason that the data require such small radii is that the drop from the blue wing of the iron line is at ∼8.5 keV (Fig. 4), so requiring large Doppler blueshifting from the rest line energy for He-like iron (as implied by the ionization state) of 6.7 keV.

At first sight this strongly supports the untruncated disc. However, the parameters are puzzling in this geometry. The amount of reflection is very small, which, together with the hard continuum, supports models where the X-rays are beamed away from the disc (e.g. Malzac, Beloborodov & Poutanen 2001). However, this also changes the illuminating radiation pattern, defocusing it away from the disc central regions. Yet the reflection spectrum requires that the inner disc is illuminated in order to produce the observed smearing. This, together with the fact that the features being fit by reflection are very small (less than a few per cent in a ratio plot), means that they are critically dependent on the current calibration of the *XMM–Newton* EPIC-pn timing mode. We explore this in more detail below by using a combination of all the low/hard state spectra, and the Crab data.

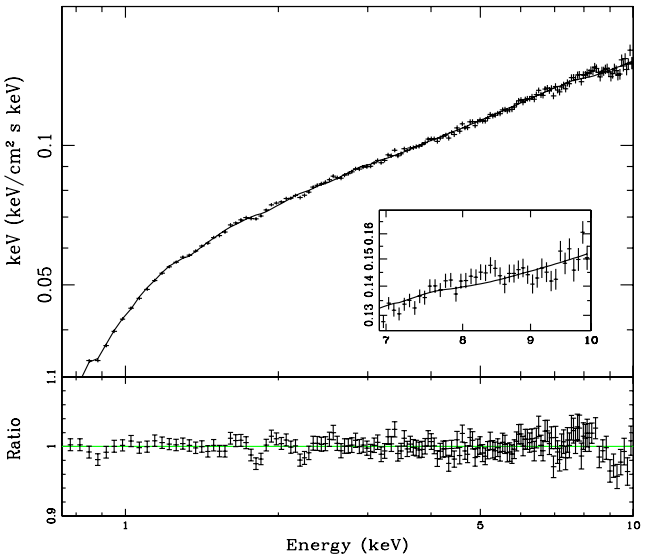

Figure 4. The S1753 observation modelled with a simple DISKBB+NTHCOMP continuum plus reflection, and zoomed in to the 7–10 keV region. An ∼6 per cent dip is visible in the residuals at ∼9 keV.

5 ALL LOW/HARD STATE SPECTRA AND LIMITATIONS OF THE CURRENT EPIC-PN TIMING MODE RESPONSE

We fit all the spectra with a continuum model of a disc plus single Comptonization model, i.e. assume that there is a real additional soft component. This is supported by the fact that Cyg X-1 and GX1,2,3 all have similar lag spectra to S1753 (GX4 is too recent an observation to be included in Uttley et al. 2011). Figs 1 and 2 show that all the spectra, apart from S1753, have obvious residuals from reflection, so we also include reflection in the model TBABS*(DISKBB+NTHCOMP+KDBLUR*RFXCONV*NTHCOMP). Both GX 339−4 and Cyg X-1 also require a small, narrow, neutral core to the iron line, which is probably due to reflection from the raised rim of the outer disc. We include this as a narrow (σ fixed to 0.01 keV) neutral line (energy fixed at 6.4 keV) in the model. All our fit parameters are shown in Table 2 and residuals are plotted in Fig. 5.

The residuals to the best-fitting models clearly show increasing problems around the edges in the response matrix (∼1.8 and ∼2.2 keV) as the source count rate increases, presumably due to the uncorrected effect of XRL. However, spectrum GX3, taken 1 d after spectrum GX2 (consecutive *XMM–Newton* orbits) and with very similar count rate and spectral shape, has stronger residuals at 2.2 keV, indicating a different gain shift. This cannot be due to different XRL as the count rate is very similar. Instead it most likely shows the systematic uncertainty of the EPIC-pn timing mode calibration. The stronger residuals around the instrument edges affect some of the fit parameters, so that the disc normalization changes significantly. This is almost certainly an artefact, as real changes in

Table 2. Best-fitting parameters from the fits with diskbb and a single Comptonization model, assuming there is a real soft component, representative of an accretion disc. The data/model ratios are plotted in Fig. 5.

	TBABS*(DISKBB+NTHCOMP+GAUSSIAN+KDBLUR*RFXCONV*NTHCOMP)									
	$N_{\rm H}(\times 10^{22})$	$T_{\rm in}$(keV)	$N_{\rm Disc}(\times 10^{3})$	Γ	$N_{\rm comp}$	$R_{\rm in}$ (R_g)	$f=\Omega/2\pi$	logξ	eW (eV)	χ^2/d.o.f
Cyg X-1	4.8 ± 0.02	0.21 ± 0.01	170^{+40}_{-30}	1.69 ± 0.01	1.48	16 ± 4	0.07 ± 0.01	$2.80^{+0.11}_{-0.05}$	8 ± 2	294/158
GX4	6.6 ± 0.2	0.18 ± 0.01	660^{+100}_{-80}	1.58 ± 0.02	0.27	$2.2^{*}_{-0.5}$	3.54 ± 0.02	270^{*}_{-150}	8 ± 3	381/158
GX3	3.7 ± 0.01	0.31 ± 0.01	$1.6^{+0.4}_{-0.2}$	1.55 ± 0.01	0.14	92^{+35}_{-20}	$0.15^{+0.01}_{-0.02}$	$2.69^{+0.01}_{-0.11}$	5 ± 3	552/158
GX2	3.9 ± 0.2	0.27 ± 0.02	$2.6^{+0.9}_{-0.7}$	1.56 ± 0.01	0.14	85^{+40}_{-25}	0.17	$2.53^{+0.17}_{-0.08}$	5 ± 3	358/158
GX1	4.4 ± 0.2	$0.24^{+0.01}_{-0.02}$	$2.6^{+1.2}_{-0.8}$	1.53 ± 0.01	9.0	110^{+80}_{-40}	$0.17^{+0.04}_{-0.03}$	$2.37^{+0.05}_{-0.02}$	13 ± 3	154/158
S1753	$1.2^{+0.4}_{-0.2}$	$0.20^{+0.10}_{-0.05}$	$0^{+2.4}_{*}$	1.60 ± 0.01	0.05	$1.9^{+6.9}_{-0.6}$	$0.06^{+0.04}_{-0.02}$	$2.76^{+0.21}_{-0.05}$		140/159

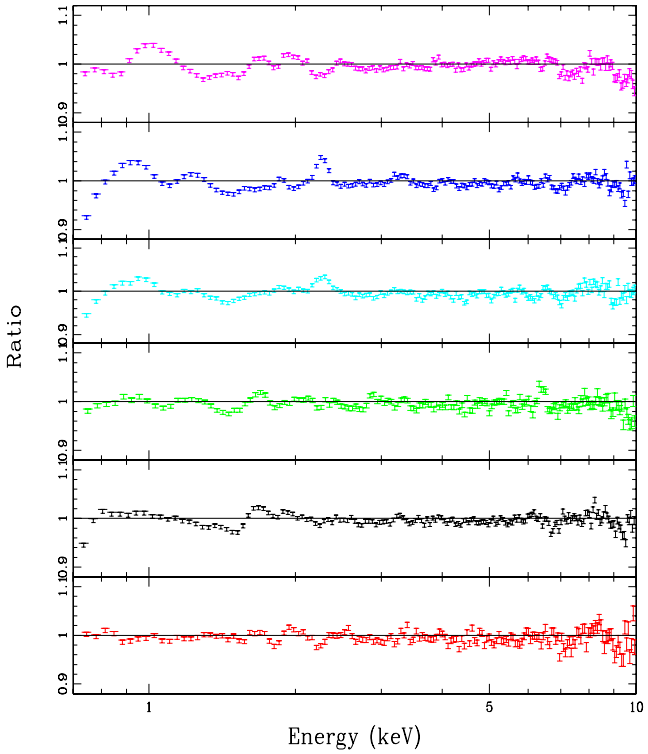

Figure 5. Data/model ratio for all spectra, when fitted with DISKBB+NTHCOMP+REFLECTION model.

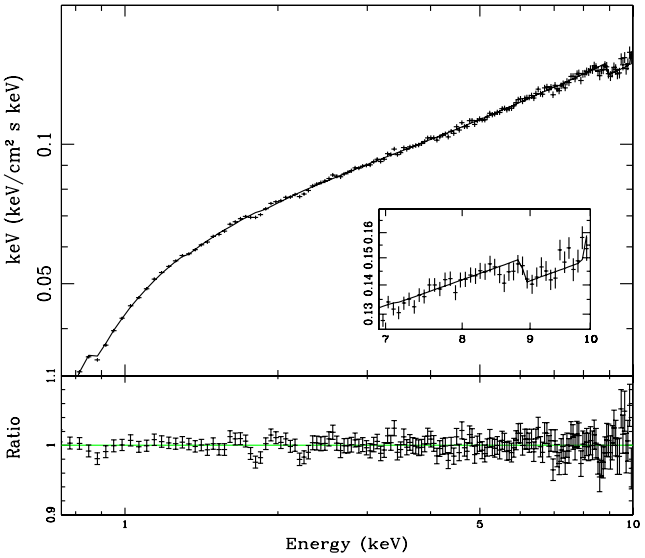

Figure 6. The S1753 observation modelled as in Fig. 4, but with a broad absorption line fixed at 9.39 keV as described in Section 3.

geometry are not likely to occur on such short time-scales without a correspondingly change in flux. Hence it seems most likely that the difference between GX2 and GX3 is driven mainly by unknown, time-dependent stability issues in the EPIC-pn response.

There is also an excess at 1 keV, which appears systematically stronger at higher $L/L_{\rm Edd}$. Such an excess is often seen in heavily absorbed systems (e.g. Hiemstra et al. 2011), where it may be a symptom of the uncertainties in the low energy tail of the response to higher energy photons. However, this should not be an issue for the low-to-moderate absorption columns required here. Thus it is likely to be real. Nonetheless, it is not easy to interpret physically, despite the energy pointing to iron L emission, as the reflector required to make the iron K line is too highly ionized to produce much iron L. A reflection origin would also impact on the lag spectrum, turning the generic hard lag into a lead at these energies as the reflected emission will follow the hard X-ray illumination (e.g. Madej & Jonker 2011). The lag spectra show no such feature (Uttley et al. 2011). Hence this most probably shows that the soft component is not well modelled by DISKBB, but instead has a more complex spectrum (see also Shidatsu et al. 2013).

There is also a drop above 9 keV which is always present. This feature could be real if there are substantial amounts of ionized H-like iron as this has a K-edge energy of 9.28 keV (e.g. Hiemstra et al. 2011). However, it would then be expected to vary with the amount of ionized reflection, yet this drop has the same ∼5 per cent level irrespective of $L/L_{\rm Edd}$. One possible explanation for this edge-like feature could be the lack of background subtraction at these high energies, rather than an intrinsic feature in the spectra. However, extracting a background in RAWX [3:10] did not make this feature disappear. The presence of a warm absorber could also result in a broad edge at these energies, as shown in e.g. Díaz Trigo et al. (2012). However, the fact that the same feature seems to be present in one of the on-axis EPIC-pn Crab observations (see the Appendix) suggests that it might be an instrumental effect.

We revisit all our spectral fits with this caveat. For S1753, the drop at high energies in the data was the key feature which meant that highly smeared reflection was significantly detected. With the NOTCH (Fig. 6), the reflection component is now only marginally significant ($\Delta\chi^2 = 12$ for three additional degrees of freedom), though all the model parameters are similar within the uncertainties. This includes the inner radius, which is still small, showing that the best-fitting model has reflection which is strongly smeared, but the

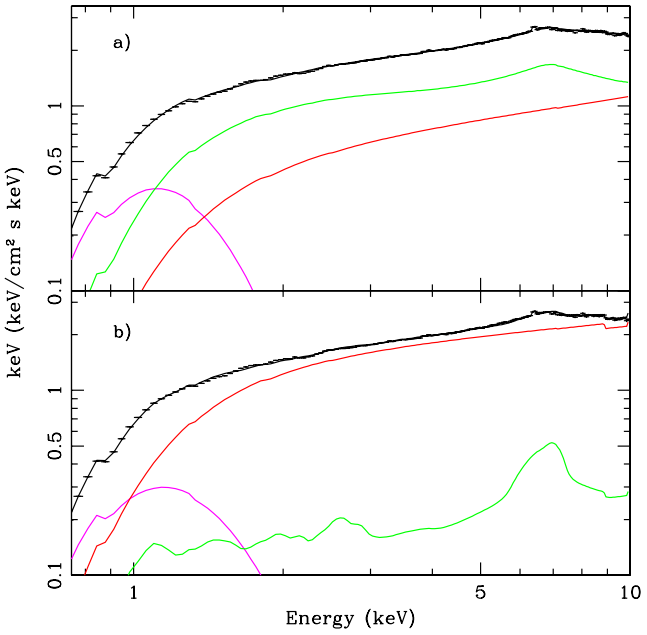

Figure 7. The spectral decomposition of GX4 without the NOTCH (top panel) and with the NOTCH (bottom panel). These two very different solutions to the data give very similar χ^2 values: 392/158 d.o.f (without notch) and 397/158 d.o.f (with notch). The green line describes the reflection component; the continuum is plotted in red and the soft component in magenta.

driver for this is now the soft excess at low energies produced by ionization reflection rather than the iron line region. We caution that there is a 30 per cent difference in the amount of low energy reflection between the Ross & Fabian (2005) calculations and the new models of García et al. (2013). Both codes calculate constant density illumination, so should be directly comparable, and give very similar results for softer spectra (García et al. 2013).

None of the fits to GX1-3 and Cyg X-1 is significantly changed by inclusion of the NOTCH, as reflection is much more significantly detected in these data sets, and is less strongly smeared in the GX 339−4 observations ($r_{\rm in,\,ref} > 100$) than in S1753. This makes it much less dependent on the high energy region, so the reflection parameters are robust to small changes in effective area at 9–10 keV.

However, for GX4, the much broader reflection features mean that the high energy calibration again makes a difference. Without the NOTCH, the amount of reflection is larger than expected for isotropic illumination, with $\Omega/2\pi = 1.3$. The spectral broadening of the iron features which is also evident in Figs 1 and 2 is driven mainly by its higher ionization state, so the derived inner radius is surprisingly large, with $r_{\rm in,\,ref} > 100$. With the NOTCH the amount of reflection drops to $\Omega/2\pi = 0.35$, its ionization is similar to that in GX1,2,3 and the obvious broadening is now due to a smaller inner radius, with $r_{\rm in,\,ref} = 50$. These very different spectral decompositions are shown in Figs 7(a) and (b).

We also note that even without the NOTCH, the spectral decomposition in Fig. 7(a) where reflection dominates the continuum in the 1–4 keV bandpass is dependent on the detailed shape of the reflected continuum in this energy range as well as on the shape of the iron line, so will also be sensitive to the reflection model uncertainties discussed in García et al. (2013). Thus the spectral decomposition in Fig. 7(a) is not robust to both current instrumental and model uncertainties.

6 DISC, DOUBLE COMPTONIZATION AND REFLECTION

The spectral lags clearly show that there is a separate soft component in S1753, GX1,2,3 and Cyg X-1 (Uttley et al. 2011). While GX4 was not included in that study, it is plain from the spectrum alone that there is a separate soft component in these data also, as $L_{\rm soft}/L_{\rm tot}$ is much larger in this data set than in the others. However, the spectral lags are not confined to the soft component alone. It has long been clear that there is a complex pattern of hard lags in Compton continuum, which requires an inhomogeneous emission region. The most successful model to date can match these observed lags by fluctuations propagating down through the accretion flow, where the outer parts of the flow have a softer spectrum than the inner. Two Comptonization components (together with the disc and reflected emission) are also required to adequately model the low/hard state spectra of BHB (Di Salvo et al. 2001; Makishima et al. 2008; Yamada et al. 2013). We describe this additional Comptonization with the COMPTT model rather than using another NTHCOMP component so that we can more easily keep track of each component. However, the more limited bandpass of our data means that we cannot constrain all the parameters, so we fix the electron temperature of this additional component at 10 keV. We assume that both soft and hard Compton components have the same seed photon energy, and that this represents the temperature of the disc itself.

An additional soft continuum component generically means that the disc component goes down to lower temperatures, and its normalization increases, as does the interstellar column density. This is a nice feature of this additional component, as all the columns derived from the previous fits are somewhat lower than expected, except for GX4. However, again our data cannot constrain all of the parameters, so we fix $N_{\rm H}$ at the expected value for all of our data (0.21, 0.55 and 0.55 $\times$ 10^{22} in S1753, GX 339−4 and Cyg X-1, respectively). We include the NOTCH with parameters fixed to those of the Crab, and tabulate results in Table 3.

This model gives significantly better fits than the single Compton continuum model (compare with Table 2) for all spectra except for GX4. In GX4 the observed, dominant soft component has a shape which is very similar to a disc. By contrast, in all the other spectra where the soft component makes only a small contribution to the spectrum below 1 keV, the shape of this soft component is much better described by thermal emission plus a broader spectrum. Conversely, in S1753, the combination of this broader soft emission plus the NOTCH means that reflection is not significantly detected.

7 THE CHANGING DISC INNER RADIUS

Fig. 8(a) shows the relation between the disc inner radius derived from reflection and from the soft component for the single Compton continuum models (Table 2) while Fig. 8(b) shows this for the double Compton fits. The truncated disc model predicts that the disc inner radius decreases with increasing $L/L_{\rm Edd}$ i.e. should become progressively smaller from S1753 (magenta), GX1 (green), Cyg X-1 (black), GX2-3 (cyan/blue), to GX4 (red). However, the data do not show this for either model.

With a single Compton continuum, the dimmest source requires the smallest disc in both soft emission and reflection (S1753), and the reflection radius strongly requires an untruncated disc. GX1-3 are consistent with an untruncated disc from their soft components, while their reflected emission indicates a truncated disc. By contrast, in Cyg X-1 both reflection and soft emission indicate that the disc is moderately truncated, though the derived radii are not

Table 3. Best-fitting parameters from a double Comptonization model, including the NOTCH component. This additional component, together with a broader soft emission, means reflection is not significantly detected in S1753.

	NOTCH×TBABS(DISKBB+COMPTT+NTHCOMP+GAUSSIAN+KDBLUR×RFXCONV×NTHCOMP)									
	$T_{\rm in}$ (kev)	$N_{\rm Disc}(\times 10^3)$	τ	$N_{\rm comp}$	Γ	$N_{\rm nthcomp}$	$R_{\rm in}(R_g)$	$f=\Omega/2\pi$	logξ	χ^2/ d.o.f
Cyg X-1	0.17 ± 0.01	490 ± 6	$2.3^{+0.1}_{-0.2}$	0.32	$1.40^{+0.03}_{*}$	0.56	$4.5^{+0.6}_{-0.5}$	$0.15^{+0.04}_{-0.02}$	2.72 ± 0.02	222/157
GX4	0.21 ± 0.01	140 ± 20	*	*	1.73 ± 0.01	1.1	47^{+10}_{-7}	$0.35^{\pm}0.05$	2.44 ± 0.04	381/158
GX3	0.16 ± 0.01	71^{+12}_{-9}	1.5 ± 0.1	0.044	$1.40^{+0.01}_{*}$	0.13	140^{+60}_{-50}	0.18 ± 0.03	$2.49^{+0.18}_{-0.04}$	360/150
GX2	0.16 ± 0.01	65 ± 9	1.6 ± 0.1	0.036	$1.40^{+0.01}_{*}$	0.12	115^{+85}_{-35}	0.19 ± 0.03	$2.45^{+0.07}_{-0.04}$	212/157
GX1	0.17 ± 0.01	26^{+5}_{-3}	1.8 ± 0.2	0.014	$1.40^{+0.03}_{*}$	0.07	150^{*}_{-50}	$0.17^{+0.04}_{-0.03}$	2.35 ± 0.03	150/157
S1753	$0.15^{+0.01}_{-0.04}$	$6.7^{+3.4}_{-1.0}$	2.2 ± 0.8	0.011	$1.40^{+0.1}_{*}$	0.03	*	*	*	141/161

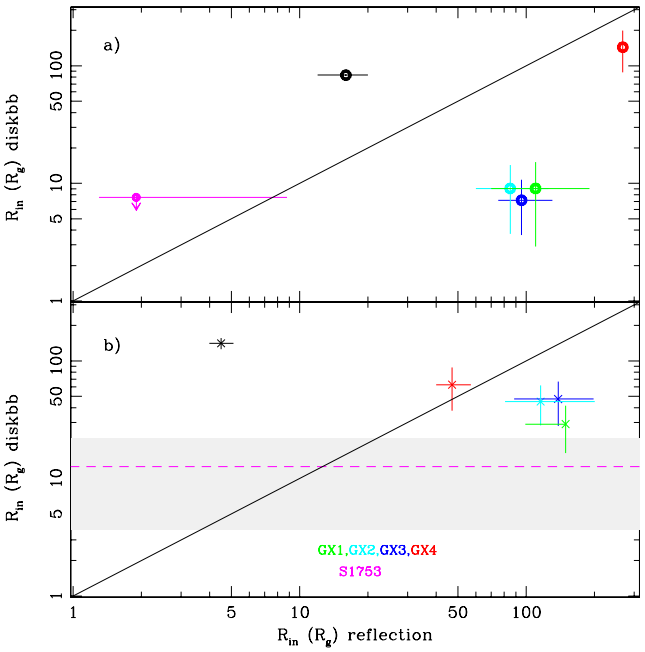

Figure 8. The relation between the disc inner radii derived from the disc normalization and reflection. The line illustrates where the points would lie if these two methods gave consistent results. (a) The inner radius derived from the soft component (Table 2). The S1753 disc normalization gives only an upper limit for $R_{\rm in}$ when measured from the soft component. (b) The inner radius derived from the reflection component (Table 3). Since reflection is not significantly detected in S1753, the dashed line shows the radius based on the disc normalization, with the grey area illustrating the error in y-direction. GX4 inner radius is the only one in our sample to show consistency within the errors.

consistent with each other. However, the soft component radius is dependent on the system parameters and for GX 339−4 we can compare the disc emission in these low/hard state data with that derived from the disc dominated state. We choose the brightest, most disc dominated observation from those of Kolehmainen et al. (2011) i.e. Obsid 0093562701 (burst mode) and derive a DISKBB normalization of $2.9 \pm 0.1 \times 10^3$. This clearly indicates the radius of the last stable orbit, and is consistent with the disc normalization seen in the GX1–2 low/hard state spectra. The disc normalization then increases quite markedly for the brighter GX4 data. If these low/hard state radii derived from the soft component are reliable the disc is not truncated for the lowest luminosity spectra, but is truncated for the brighter low/hard state of GX4, and then goes back down to the last stable orbit when the source makes a transition to the disc dominated state. Similar behaviour is also seen in XTE J1817−330 (Gierliński et al. 2008), where the constant radius soft component seen in the disc dominated state first increases in radius during the transition to the low/hard state and then decreases in the dimmer low/hard state. Gierliński et al. (2008) show that this behaviour can be consistent with the disc progressively truncating in the low/hard state as the radii derived for these data are model dependent and could be increased by irradiation, and/or a stressed boundary condition and/or an increased colour temperature correction. We also note that the disc inner radius is also increased if the Compton cloud is between the disc and observer, as photons in the Comptonized spectrum came originally from scattering of seed photons from the disc (Kubota & Done 2004).

Fig. 8(b) with radii derived from reflection and emission from the disc with a double Compton continuum (plus high energy notch for calibration) shows a rather different pattern. However, it is still inconsistent with the overall decrease in radii for brighter low/hard states predicted for the truncated disc models. The soft component in S1753 still indicates a rather small radius for the disc, smaller than the much brighter GX4 data set. However, GX1–4 now do show a marginal trend of decreasing radius from reflection with increasing $L/L_{\rm Edd}$, opposite to the increasing radius seen from their soft component normalization. However, both disc reflection and emission require that the radius is much larger than the innermost stable circular orbit. However, in Cyg X-1, the disc reflection now requires an untruncated disc, while the soft component requires a much larger radius.

We note that both Cyg X-1 and GX4 spectra were derived using central column removal. The Appendix shows that large changes around the iron line can be produced by this process using different energy-dependent PSFs. Thus the relativistic smearing parameters derived from Cyg X-1 (the most piled-up spectrum used in our analysis) are particularly suspect, while GX4 may be rather less affected. We note that issues with the iron line method were also recently discussed in Dauser et al. (2013), and Sanna et al. (2012). In the latter paper the line profile implied a physically impossible inner radius of $2.0^{+0.4}_{-0.2} R_g$ for the neutron star 4U 1636−53 (Table 1; Sanna et al. 2012).

Larger features are clearly more robust than small, so even though GX4 has central columns removed, this is not going to remove the large soft component which is clearly detected. Also, by eye, the amount of reflection shows a clear trend as a function of $L/L_{\rm Edd}$ (Fig. 1). At the lowest luminosities the iron line is not required, then reflection becomes a significant feature in the data, though with small solid angle $\Omega/2\pi \sim 0.2$. This reflecting material is significantly ionized. For bright low/hard states (GX4) reflection

is much stronger, and much more obviously broadened. This is all consistent with the truncated disc models. What is not, however, is the smaller radius inferred for the soft component in the lower luminosity spectra GX1-2 and S1753, though we note that this still implies a truncated disc in the double Compton continuum models. Instead, we suggest that this component is from small clumps torn from the disc edge as it truncates, forming a small, variable soft component while the true truncated disc emission is outside of the bandpass (though it can be seen directly in the lower absorption system XTE J1118+480: Esin et al. 2001) As the mass accretion rate increases, the truncated disc extends closer to the black hole and can be seen directly, though there are probably still some residual variable clumps which contribute to the spectrum (see also Chiang et al. 2010; Yamada et al. 2013).

8 CONCLUSIONS

We present an analysis of the inner disc radius in the low/hard state of BHBs as measured by both disc emission and reflection, carefully considering instrumental uncertainties as both features are typically rather small. The limitations of the current calibration are important to consider, as BHBs are extremely bright. This necessitates the use of the timing (or burst) mode, where the systematics are not so well understood, yet the excellent quality of the data means that the data are typically limited by systematics rather than statistics.

We highlight some calibration issues, such as uncertainties in the energy dependence of the off-axis spectral response which become important for piled up spectra where the central columns are removed. Different energy dependencies in the PSF give grossly different spectra around the iron line. We caution that this aspect of timing mode is not currently well enough calibrated to constrain small features such as the smearing of the reflected emission. This affects data sets GX4 and especially Cyg X-1 in our analysis. Cyg X-1 is the only low/hard state timing mode observation which requires an untruncated disc as measured by the reflected spectrum.

We also discuss the status of the high energy calibration above $\sim$9 keV, an uncertainty which is compounded by the cross-calibration offset of $\Delta\Gamma = 0.15$ with the *RXTE* PCA in their overlapping bandpass of 3–10 keV, which means that they cannot be reliably fit together. A small change in the effective area above $\sim$9 keV can dramatically change the inferred reflected parameters for strongly smeared reflection. This affects both S1753 and GX4 in our analysis. For S1753, where the standard response shows that reflection is very small but extremely smeared, a small change in the high energy response (along with a more physically realistic continuum model) can remove the requirement for any reflected component. Conversely, for GX4, a similarly small change can dramatically reduce the amount of reflection, switching the solution from being reflection dominated to having only a small amount of reflection. The iron line is strongly smeared in these data, but the models identify this as being mainly due to ionization rather than velocity.

Conversely, observations where reflection is unambiguously detected but does not dominate the spectra and is not highly smeared (i.e. GX1, 2 and 3), the reflection parameters appear to be fairly robust to these calibration issues.

The blackbody component is significantly detected in all data sets irrespective of calibration issues, except in S1753. However, in all these data, including S1753, the blackbody is independently required by the difference in timing properties at the lowest energies (Wilkinson & Uttley 2009). We show that the derived inner disc radius is sensitive to details of the continuum spectral model, especially in S1753 where there is a strong upper limit to the disc radius with a single Compton continuum, but where it is much larger with the double Compton model which is required to produce the continuum spectral lags (e.g. Wilkinson & Uttley 2009).

However, even the double Compton model gives inferred inner radii which are somewhat smaller in the lower luminosity spectra (S1753 and GX1-3) than in GX4 though the radii are still large enough to require the disc to be truncated. This could signal a change in the nature of the soft component from small variable clumps when the disc is truncated far from the black hole to the truncated disc itself when it extends close enough to the black hole in the bright low/hard states for this constant emission to contribute to the low energy bandpass.

In summary, these EPIC-pn timing mode low/hard state data do challenge the truncated disc models, but there are both model uncertainties and calibration uncertainties which mean that the challenges can be incorporated by extending the standard, very successful, truncated disc model rather than abandoning it. In general, we caution that both reflection and the disc blackbody are small features in this state, so are dependent on the details of the instrument calibration as well as on the spectral models used. We strongly support the on-going effort by the *XMM–Newton* team to improve the current calibration and cross-calibration status of the EPIC-pn.

ACKNOWLEDGEMENTS

We would like to thank Matteo Guainazzi for all the extensive discussions on *XMM–Newton* data reduction and calibration issues during this project. MK also acknowledges an STFC postdoctoral grant and the support of the Vilho, Yrjö and Kalle Väisälä Foundation from the Finnish Academy of Science.

This work is based on observations obtained with *XMM–Newton*, an ESA science mission with instruments and contributions directly funded by ESA Member States and NASA.

REFERENCES

Arévalo P., Uttley P., 2006, MNRAS, 367, 801
Axelsson M., Hjalmarsdotter L., Done C., 2013, MNRAS, 431, 1987
Chiang C. Y., Done C., Still M., Godet O., 2010, MNRAS, 403, 1102
Churazov E., Gilfanov M., Revnivtsev M., 2001, MNRAS, 321, 759
Dauser T., Garcia J., Wilms J., Bock M., Brenneman L. W., Falanga M., Fukumura K., Reynolds C. S., 2013, MNRAS, 430, 1694
Díaz Trigo M., Sidoli L., Boirin L., Parmar A. N., 2012, A&A, 543, A50
Di Salvo T., Done C., Życki P. T., Burderi L., Robba N. R., 2001, ApJ, 547, 1024
Done C., Díaz Trigo M., 2010, MNRAS, 407, 2287
Done C., Gierliński M., Kubota A., 2007, A&AR, 15, 1 (DGK07)
Esin A. A., McClintock J. E., Narayan R., 1997, ApJ, 489, 865
Esin A. A., McClintock J. E., Drake J. J., Garcia M. R., Haswell C. A., Hynes R. I., Muno M. P., 2001, ApJ, 555, 483
Fabian A. C., Iwasawa K., Reynolds C. S., Young A. J., 2000, PASP, 112, 1145
Fender R. P., Belloni T. M., Gallo E., 2004, MNRAS, 355, 1105
García J., Dauser T., Reynolds C. S., Kallman T. R., McClintock J. E., Wilms J., Eikmann W., 2013, ApJ, 768, 146
Gierliński M., Done C., Page K., 2008, MNRAS, 388, 753
Hiemstra B., Méndez M., Done C., Díaz Trigo M., Altamirano D., Casella P., 2011, MNRAS, 411, 137
Kawabata R., Mineshige S., 2010, PASJ, 62, 621
Kolehmainen M., Done C., Díaz Trigo M., 2011, MNRAS, 416, 311
Kotov O., Churazov E., Gilfanov M., 2001, MNRAS, 327, 799
Kubota A., Done C., 2004, MNRAS, 353, 980

Kubota A., Tanaka Y., Makishima K., Ueda Y., Dotani T., Inoue H., Yamaoka K., 1998, PASJ, 50, 667
Kubota A., Done C., Davis S. W., Dotani T., Mizuno T., Ueda Y., 2010, ApJ, 714, 860
Laor A., 1991, ApJ, 376, 90
McClintock J. E., Remillard R. A., 2006, Compact Stellar X-ray Sources. Cambridge University Press, Cambridge
Madej O. K., Jonker P. G., 2011, MNRAS, 412, L11
Makishima K. et al., 2008, PASJ, 60, 585
Malzac J., Beloborodov A. M., Poutanen J., 2001, MNRAS, 326, 417
Markwardt C. B., Barthelmy S. D., Evans P. A., Swank J. H., 2009, Astron. Telegram, 2261, 1
Miller J. M., Homan J., Steeghs D., Rupen M., Hunstead R. W., Wijnands R., Charles P. A., Fabian A. C., 2006, ApJ, 653, 525
Miller J. M. et al., 2010, ApJ, 724, 1441
Miyamoto S., Kitamoto S., Mitsuda K., Dotani T., 1988, Nat, 336, 450
Ng C., Díaz Trigo M., Cadolle Bel M., Migliari S., 2010, A&A, 522, A96
Read A. M., Rosen S. R., Saxton R. D., Ramirez J., 2011, A&A, 534, A34
Reis R. C., Fabian A. C., Miller J. M., 2010, MNRAS, 402, 836
Revnivtsev M., Gilfanov M., Churazov E., 1999, A&A, 347, L23
Ross R., Fabian A. C., 2005, MNRAS, 358, 211
Rykoff E. S., Miller J. M., Steeghs D., Torres M. A. P., 2007, ApJ, 666, 1129
Sanna A., Méndez M., Belloni T., Altamirano D., 2012, MNRAS, 424, 2936
Shidatsu M. et al., 2011, PASJ, 63, 785
Tsujimoto M. et al., 2011, A&A, 525, A25
Uttley P., Wilkinson T., Cassatella P., Wilms J., Pottschmidt K., Hanke M., Böck M., 2011, MNRAS, 414, L60
Weisskopf M. C., Guainazzi M., Jahoda K., Shaposhnikov N., O'Dell S. L., Zavlin V. E., Wilson-Hodge C., Elsner R. F., 2010, ApJ, 713, 912
Wilkinson T., Uttley P., 2009, MNRAS, 397, 666
Yamada S. et al., 2009, ApJ, 707, L109
Yamada S., Makishima K., Done C., Torii S., Noda H., Sakurai S., 2013, PASJ, 65, 80
Zdziarski A. A., Johnson W. N., Magdziarz P., 1996, MNRAS, 283, 193

APPENDIX A: THE LEVEL OF CALIBRATION UNCERTAINTIES IN THE EPIC-PN

A1 Point spread function

The SAS v12.0.1. includes an update for the way the PSF is calculated in the ARFGEN task. The previous 'EXTENDED' PSF model is replaced with a new, two-dimensional 'ELLBETA' model (Read et al. 2011) as a default setting. We compared these new responses to the ones generated with SAS v10.0, and found that the spectral shape seemed to change noticeably in the two piled-up observations GX4 and Cyg X-1 (see Fig. A1 for the GX4 comparison). Further investigation into this discrepancy showed that the 'ELLBETA' model indeed has issues at large radii in the timing mode, which become more pronounced when the central RAWX columns are excised to correct for pileup. The deviation is most noticeable in the iron line region, between ∼4 and 8 keV, and therefore makes a significant difference in any analysis of the reflection features. However, manually setting psfmodel=EXTENDED when running ARFGEN brings the spectral curvature and the residuals back to a level that is consistent with the previous versions of SAS. It is not clear which of these two models better represents the true energy dependence of the PSF.

A2 Crab calibration

We also take a closer look at the drop above 9 keV that is visible in all of our observations using Crab data. Fig. A2 shows a series of residuals from spectral fits to one of the on-axis observations of the Crab (see Appendix). The top panel shows residuals to a

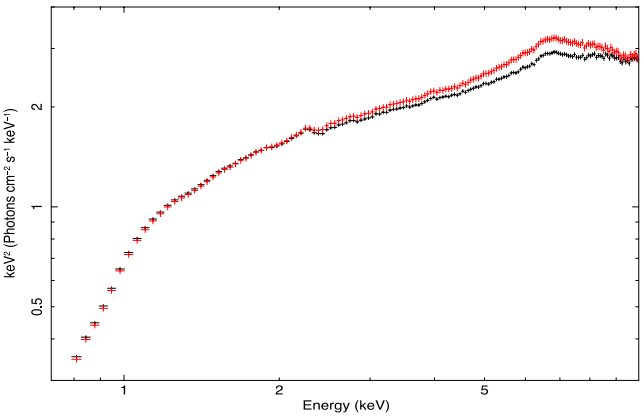

Figure A1. GX4 spectra, extracted with SAS v12.0.1. and corrected for pileup by ignoring the central RAWX columns. The black spectrum was extracted using psfmodel=extended, whereas the red spectrum shows the default setting psfmodel=ellbeta. The difference is most pronounced in the iron line region, and the spectral curvature changes above ∼7.5 keV.

single power law, with $\Gamma = 2.1$. This is a similar fit to those in Weisskopf et al. (2010), but here the more appropriate binning does not suppress the visibility of the high energy residuals. There are clear residuals below 1.5 keV and at 9 keV, which appear fairly similar to the ones in our data (Fig. A2a). However, a single power law is not a good approximation to the spectrum from the Crab, as there are both nebular and pulsar contributions. Instead, a double power-law fit removes the soft residuals, but not the high energy feature at 9 keV (middle panel). We model this with a NOTCH, with width fixed at 1 keV and find a significant reduction in χ^2 (from

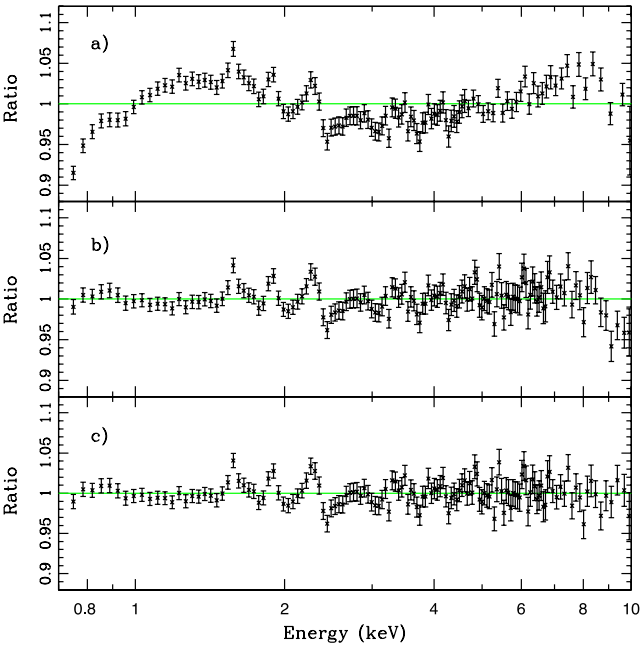

Figure A2. Upper panel (a): Residuals from a double power-law model of the Crab with EPFAST correction. The features between ∼1.6 and 2.4 keV are due to the CTI correction, which seems to have over-compensated the characteristically negative residuals. (Middle panel b): A double power-law model to account for both nebular and pulsar contributions to the observed spectrum removes the dip at low energies. (Lower panel c): Residuals from the same double power-law model as the middle panel, with the additional NOTCH absorption line fitted at 9.39 keV.

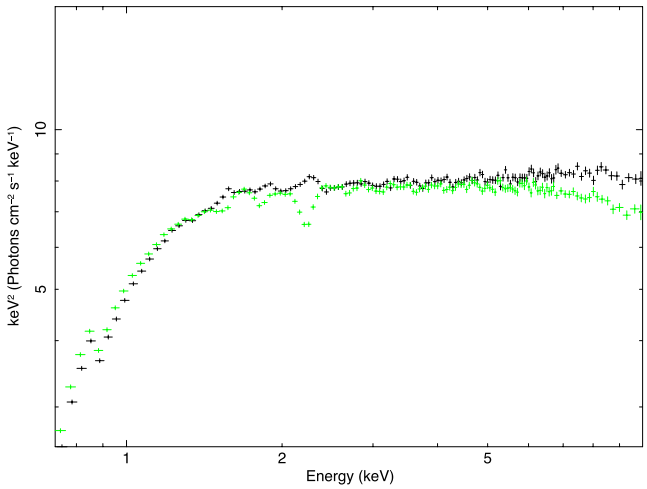

Figure A3. Crab observation 01610960401 with EPFAST correction (in black) and without (in green). The rate-dependent CTI effects are visible in the non-corrected data, whereas the corrected one shows over-compensation around the instrumental Si and Au edges.

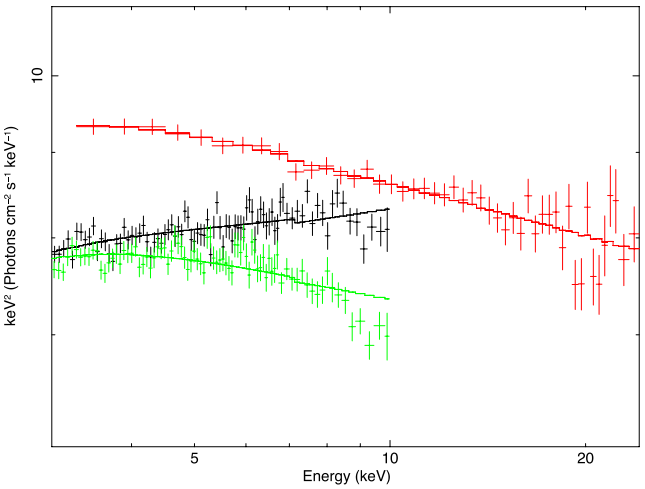

Figure A4. Same as Fig. A3, combined with the corresponding PCA observation in red. EPFAST has corrected for the turnover above ∼8 keV in the non-corrected data, but rather over-estimated the instrumental edges at ∼1.85 and ∼2.2 keV.

260/162 to 231/160) for an energy 9.39 ± 0.01 keV, with a covering fraction of 0.06 ± 0.02 (i.e. equivalent width 60 eV). The residuals in Fig. A2(c) are now flat. However, this feature is not significantly present in the other on-axis Crab spectrum, so we regard this instead as showing the limitations of our current knowledge of the response.

A3 Limits from cross-calibration with RXTE

One way to assess the status of the cross-calibration between the EPIC-pn fast timing mode and PCA is to use Crab data, though this is necessarily in pn burst mode rather than timing mode due to the very high count rate of the Crab. Essentially, features seen in the spectra of BHBs are not expected to be found in the Crab. Thus we tried to shed more light into the very concerning cross-calibrational disagreement seen in Fig. 3 by comparing EPIC-pn and PCA observations of the Crab. However, due to the brightness of the Crab, most of the *XMM–Newton* observations are taken in a slightly offset position. There are only two archived EPIC-pn burst mode observations (01610960401 and 0160960601) that were taken in a bore-sight position, thus allowing the whole nebula to be fully encompassed by the aperture (CAL- TN-0083).

We coupled the pn observation 01610960401 with a PCA observation (90802-02-05-00), taken 5 d prior to the *XMM–Newton* one. Since it seems that the rate-dependent CTI correction task EPFAST does not properly correct for these pn Crab spectra (see Fig. A3 and features around 2 keV in Fig. A2), we considered both EPFAST-corrected and non-corrected pn spectra for the comparison. Fig. A4 shows the data fitted with an absorbed two-component power law, with the EPFAST-corrected EPIC-pn data in black, non-corrected in green and the PCA in red. The difference in photon index is blatantly evident even by eye, and fitting the spectra in the combined energy range of 0.7–25 keV gives a difference in photon index of $\Delta\Gamma = 0.16 \pm 0.01$ between the CTI-corrected pn and the PCA spectra. We tested this further by fitting only above 3 keV to omit any absorption effects that might affect the pn spectra at low energies. This yielded individual indices of $1.97^{+0.03}_{-0.06}$ for the EPFAST-corrected EPIC-pn, 2.14 for the non-corrected pn and 2.12 for the PCA. Thus, the EPFAST-corrected spectrum shows stronger disagreement with the PCA, whereas the non-corrected spectrum rolls over above ∼8 keV in a way that wrongly resembles the PCA spectral index. In addition, the absorption feature seen in Fig. A2 is even greater in a non-corrected spectrum, with a >15 per cent residual at 9 keV.

A discrepancy this noticeable is obviously very concerning. One possibility is that it could be due to an incorrect energy-dependency of the rate-dependent CTI and the calibration effort in currently on-going. However, dealing with a burst mode observation of the Crab nebula is complex in itself. None of the data reduction and/or analysis choices is trivial. Issues such as centralizing the extraction region at the peak of the emission in RAWX, the size of the extraction region and subtracting a background from the source all affect the resulting spectrum. It is also currently impossible to correct for the unknown universal effect of XRL in the data.

However, the issue is not just seen in timing and burst mode spectra. The cross-calibration source for standard imaging mode, G21.5–0.9, shows the same discrepancy when fit in the 3–10 keV region of overlap. These data are analysed in the comprehensive cross-calibration paper of Tsujimoto et al. (2011), but he compared data sets in the overlapping 2–10 keV bandpass, and so did not include a high energy PCA-pn comparison. However, he kindly provided his data to us, and we restrict the bandpass of both to 3–10 keV and find $\Gamma = 2.00 \pm 0.01$ for the PCA, with $\Gamma = 1.85^{+0.01}_{-0.03}$ for the pn for these imaging mode data.

All these factors in mind, we conclude that the discrepancy in cross-calibration limits joint EPIC-pn/PCA spectral fitting in all modes.

This paper has been typeset from a TEX/LATEX file prepared by the author.